

Effects of pulsatile blood flow in large vessels on thermal dose distribution during thermal therapy

Tzyy-Leng Horng

Department of Applied Mathematics, Feng Chia University, Taichung, Taiwan

Win-Li Lin

Institute of Biomedical Engineering, National Taiwan University, Taipei, Taiwan and Medical Engineering Research Division, National Health Research Institutes, Miaoli, Taiwan

Chihng-Tsung Liauh

Department of Mechanical Engineering, Kun Shan University of Technology, Tainan, Taiwan

Tzu-Ching Shih^{a)}

Department of Medical Radiology Technology, China Medical University and Department of Radiology, China Medical University Hospital, Taichung, Taiwan

(Received 1 November 2006; revised 3 February 2007; accepted for publication 6 February 2007; published 16 March 2007)

The aim of this study is to evaluate the effect of pulsatile blood flow in thermally significant blood vessels on the thermal lesion region during thermal therapy of tumor. A sinusoidally pulsatile velocity profile for blood flow was employed to simulate the cyclic effect of the heart beat on the blood flow. The evolution of temperature field was governed by the energy transport equation for blood flow together with Pennes' bioheat equation for perfused tissue encircling the blood vessel. The governing equations were numerically solved by a novel multi-block Chebyshev pseudospectral method and the accumulated thermal dose in tissue was computed. Numerical results show that pulsatile velocity profile, with various combinations of pulsatile amplitude and frequency, has little difference in effect on the thermal lesion region of tissue compared with uniform or parabolic velocity profile. However, some minor differences on the thermal lesion region of blood vessel is observed for middle-sized blood vessel. This consequence suggests that, in this kind of problem, we may as well do the simulation simply by a steady uniform velocity profile for blood flow. © 2007 American Association of Physicists in Medicine. [DOI: [10.1118/1.2712415](https://doi.org/10.1118/1.2712415)]

Key words: pulsatile blood flow, bioheat transfer, thermal dose, Chebyshev pseudospectral method

I. INTRODUCTION

Blood flow can remarkably affect the temperature distributions in tumor tissues during thermal therapies, especially with the presence of large blood vessels.¹⁻⁶ Thermally significant blood vessels (larger than 0.2 mm in diameter) cool tissue during thermal treatments, making it very difficult to cover the whole tumor volume with therapeutic thermal exposure.⁷⁻⁹ Shih *et al.*⁹ found that the short-duration high-intensity heating can treat a target tumor inside with a blood vessel diameter of 0.2 mm when using the total power energy density up to 120 J cm^{-3} . Moreover, Becker and Kuznetsov⁷ found that the target region tissue was found to have a lower thermal damage in the presence of a blood vessel, and this cooling effect is more pronounced as the blood vessel gets larger (larger than 0.6 mm in diameter). These phenomena motivated us to thoroughly study the effects of thermally significant blood vessels on thermal therapy of tumor.

The cyclic nature of the heart pump generates pulsatile blood flow in all arteries.¹⁰⁻²⁰ This periodic-in-time velocity profile for pulsatile blood flow, driven by an oscillating pressure gradient, inside a circular blood vessel was first studied by Womersley.²⁰ Loudon and Tordesillas²¹ used dimensionless Womersley number to characterize the pulsatile fre-

quency of blood flow. They showed that when Womersley number is small, the flow tracks the oscillating pressure gradient faithfully and the velocity profile exhibits a parabolic shape. Nevertheless, when Womersley number is large, the phase difference between velocity and pressure gradient becomes larger and the velocity profile exhibits a shape of two peaks.

Generally in hyperthermia treatment of tumors, blood vessels with a diameter larger than 0.5 mm can no longer be included in blood perfusion and must be treated individually²²⁻²⁶ because temperature difference between blood and surrounding tissue is significant. Heat transfer in tissue within the region near a large blood vessel is especially influenced significantly by the flowing blood.^{27,28} Furthermore, Mohammed and Verhey²⁸ utilized a finite element method to simulate laser interstitial thermo therapy on anatomical inhomogeneous regions by considering blood perfusion only and also performed in *in vitro* experiment on porcine muscle tissue. Their numerical results had 5% to 20% discrepancy in thermal lesion compared with the experiment. This indicates the importance of an appropriate thermal model to achieve reliable results from numerical simulations.

So far no numerical result considering the coupled heat transfer problem of both a large blood vessel with pulsatile

blood flow inside and its surrounding tissue is ever reported, and the whole physics remains poorly understood. Craciunescu and Clegg¹⁵ numerically solved the axis-symmetric Navier-Stokes equations to obtain the pulsatile velocity profile and then computed the energy transport equation to obtain the temperature distribution of pulsating blood flow in a blood vessel with sizes of aorta, large arteries, terminal arterial branches, and arterioles. Some cases of their simulation have pulsation of large amplitude such that reversal of blood flow occurs in large vessels (i.e., 3 mm in diameter and larger). However, they only focused on the temperature distribution within a blood vessel and did not consider that for its surrounding tissue. Shih *et al.*⁸ computed the coupled heat transfer problem of both a large blood vessel and its surrounding tissue. However, they only assumed the velocity profile of the blood flow inside the vessel to be simply steady and uniform. They found that the thermal dose would be insufficient for treatment in the region near blood vessel when the radius and flow rate are large. Shih *et al.*⁹ extended Shih *et al.*⁸ to investigate the influence of various heating speeds with the total heat applied held equal and found the thermal dose deficit in the region near blood vessel is less severe when the heating speed is large. Here we studied this coupled heat transfer problem between a thermally significant blood vessel and its surrounding tissue during heat treatment by considering the velocity profile of the blood flow being uniform, parabolic, and pulsatile under various radii of vessel, pulsating frequencies and amplitudes (in the case of pulsatile velocity profile), and heating speeds. The main object is to realize the effects of flow velocity profile, size of vessel, flow rate, and heating speed on thermal dose distribution of the surrounding tissue during heat treatment. Though many factors about blood vessels have been brought into consideration in the current study compared with existing literatures, it is still far from being complete. Many other factors such as vessel wall elasticity, porosity, rheology of blood, realistic shape of blood pressure wave, possible counter current flow, and even turbulence in pulsatile blood flow are either ignored or simplified in the current study.^{11,12,29} Here the whole paper is organized as follows: the mathematical model and its governing equations followed by its numerical method are described in the section of mathematical model and numerical method. The numerical results are presented in the section of results and discussions with the effects of flow velocity profile, size of vessel, flow rate, and heating speed on thermal dose distribution discussed. The final section is conclusion to summarize all key physics in this study.

II. MATHEMATICAL MODEL AND NUMERICAL METHOD

A. Velocity profile of pulsatile blood flow in a circular blood vessel

Besides being simply steady uniform or parabolic, the pulsation of blood flow is considered here and its velocity profile is derived as follows. Here, we assume the blood flow to be incompressible, laminar and Newtonian obeying

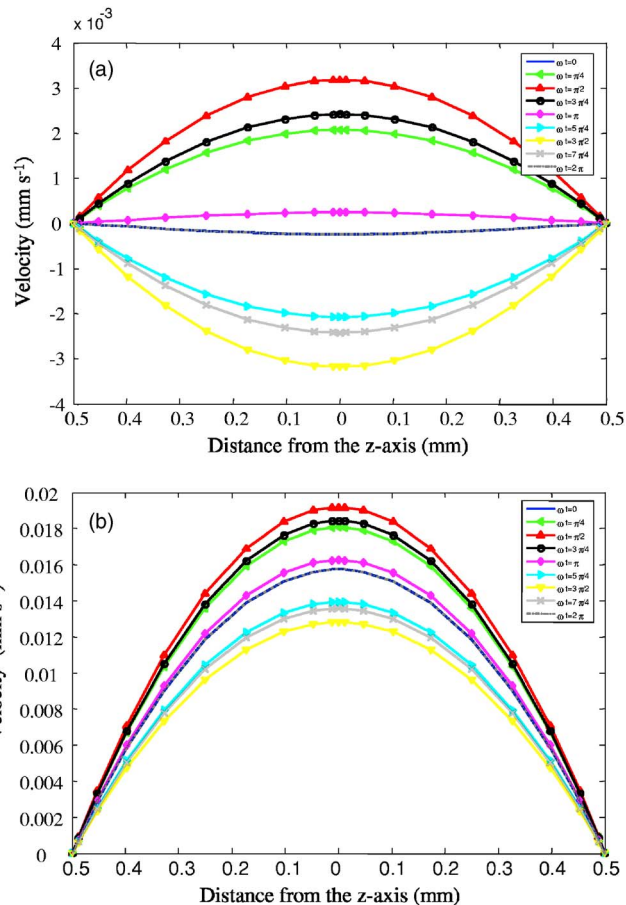


FIG. 1. Velocity profile of pulsatile blood flow at different phases for $r_0 = 0.5$ mm, $f = 1$ Hz, $\alpha = 0.64213$, $fac = 0.2$. (a) oscillating part of total velocity, (b) total velocity.

Navier-Stokes equations in a cylindrical impermeable blood vessel with rigid wall of radius r_0 . The axial Hagen-Poiseuille steady parabolic velocity profile is¹²

$$w = -\frac{1}{4\mu}(r_0^2 - r^2)\frac{dp}{dz}. \tag{1}$$

For pulsatile flows, the pressure gradient above is no more a constant, and is in fact periodic in time due to the rhythmic nature of beating heart. To mimic the realistic shape of pressure gradient in time, it requests at least 11 harmonics,²⁹ and here we simply consider the fundamental one only for the feasibility of analysis. With this additional sinusoidal component in time, the corresponding pressure gradient, without loss of major physics, along the z -axis of blood vessel can be assumed periodically as

$$\begin{aligned} \frac{\partial p}{\partial z} &= c_0 + c_1 \sin \omega t \\ &= c_0 + c_1 \frac{e^{i\omega t} - e^{-i\omega t}}{2i} \\ &= c_0 + \hat{c}_1 e^{i\omega t} + \hat{c}_{-1} e^{-i\omega t}, \end{aligned} \tag{2}$$

where $\omega = 2\pi f$ is the angular frequency; the period is denoted as $T = 1/f$; $\hat{c}_1 = c_1/2i$, $\hat{c}_{-1} = -c_1/2i$. The corresponding axial

velocity profile $W(r, t)$ can be similarly expressed in the form as

$$W = w + w_1 e^{i\omega t} + w_{-1} e^{-i\omega t}, \tag{3}$$

with $w = -1/4\mu(r_0^2 - r^2)c_0$ by Eq. (1). The volume flow rate averaged over the period T is

$$\dot{Q}_{\text{avg}} = \frac{2\pi}{T} \int_0^T \int_0^{r_0} W r dr dt = -\frac{\pi r_0^4}{8\mu} c_0, \tag{4}$$

and the average velocity in space and time is, therefore,

$$\bar{w} = \frac{\dot{Q}_{\text{avg}}}{\pi r_0^2} = -\frac{c_0 r_0^2}{8\mu}. \tag{5}$$

The velocity profile can then be further expressed as

$$W = 2\bar{w} \left(1 - \frac{r^2}{r_0^2} \right) + w_1 e^{i\omega t} + w_{-1} e^{-i\omega t}. \tag{6}$$

The sinusoidal components w_1 and w_{-1} can be determined by solving Navier-Stokes equations, and Eq. (6) can be expressed as follows by Fung:¹²

$$\begin{aligned} W &= 2\bar{w} \left(1 - \frac{r^2}{r_0^2} \right) + w_1 e^{i\omega t} + w_{-1} e^{-i\omega t} \\ &= 2\bar{w} \left(1 - \frac{r^2}{r_0^2} \right) + \frac{i\hat{c}_1}{\rho\omega} \left[1 - \frac{J_0\left(\alpha \frac{r}{r_0} i^{3/2}\right)}{J_0\left(\alpha \frac{r}{r_0} i^{3/2}\right)} \right] e^{i\omega t} - \frac{i\hat{c}_{-1}}{\rho\omega} \left[1 - \frac{J_0\left(\alpha \frac{r}{r_0} i^{5/2}\right)}{J_0\left(\alpha i^{5/2}\right)} \right] e^{-i\omega t} \\ &= 2\bar{w} \left(1 - \frac{r^2}{r_0^2} \right) + \frac{c_1}{2\rho\omega} \left[1 - \frac{J_0\left(\alpha \frac{r}{r_0} i^{3/2}\right)}{J_0\left(\alpha \frac{r}{r_0} i^{3/2}\right)} \right] e^{i\omega t} + \frac{c_1}{2\rho\omega} \left[1 - \frac{J_0\left(\alpha \frac{r}{r_0} i^{3/2}\right)}{J_0\left(\alpha \frac{r}{r_0} i^{3/2}\right)} \right] e^{-i\omega t} \\ &= 2\bar{w} \left(1 - \frac{r^2}{r_0^2} \right) + \frac{c_1}{\rho\omega} \operatorname{Re} \left\{ \left[1 - \frac{J_0\left(\alpha \frac{r}{r_0} i^{3/2}\right)}{J_0\left(\alpha \frac{r}{r_0} i^{3/2}\right)} \right] e^{i\omega t} \right\}, \end{aligned} \tag{7}$$

where

$$\alpha = \frac{r_0}{\sqrt{\nu/\omega}}$$

denotes the Womersley number; ρ and ν the density and kinematic viscosity of blood, respectively; $\operatorname{Re}(\cdot)$ the real part; J_0 is the Bessel function of the first kind of order zero. Also, we denote here

$$fac = c_1/c_0 = c_1 / \left(-\frac{8\mu\bar{w}}{r_0^2} \right)$$

to characterize the relative intensity of pulsation in blood flow. In current study, the value of fac ranges from 0.2 to 1, that is not too large to cause reverse flow judging from possible practical situations. The Womersley number α is used to describe the competition between transient inertia force and viscous force. If the Womersley number α is large, the effect of viscosity cannot propagate far from the wall, and the flow in the central portion of tube acts like inviscid flow and is chiefly determined by the balance of inertia force and pressure gradient. On the other hand, when the Womersley number α is large, the velocity profile in a pulsatile flow is

expected to be relatively blunt compared with the steady parabolic profile of Poiseuille flow. When Womersley number α is larger, the pulsating velocity profile may even have two peaks. However, this two-peak velocity profile did not occur in the current study considering the vessel diameter used here ranging from 0.2 to 2 mm and heart beat frequency 1 to 2 Hz that makes maximum Womersley number 1.8162 only. Figures 1(a) and 1(b) show the velocity profile of oscillating component and the total, respectively, for various phases in a complete cycle for a typical case in the current study ($r_0=0.5$ mm, $f=1$ Hz, $\alpha=0.642$ 13, $fac=0.2$). Neither two-peak behavior nor reverse flow is observed in the velocity profile.

B. Governing equations

Here we assume that the absorbed power density in blood and tissue is equal to the heating power density. The axis-symmetric geometric configuration considered here is a cylindrical perfused tissue, including tumor and normal tissues, with a coaxial rigid blood vessel inside and throughout the tissue as shown in Fig. 2. The whole computational domain is bounded by $r=r_{\text{max}}$, $z=0$, and $z=z_{\text{max}}$; the blood vessel is

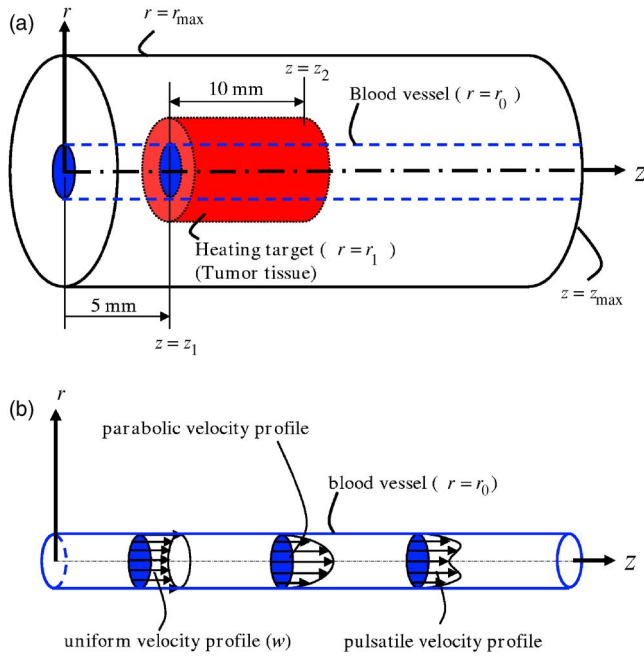


FIG. 2. Geometric configuration in current simulations. (a) The treatment target (heating target) is specified as $z_1 \leq z \leq z_2$, $0 \leq r \leq r_1$, with $z_1=5$ mm, $z_2=15$ mm, $r_1=5$ mm considered here. (b) Schematic illustration of the three kinds of velocity profile of blood flow in blood vessels. Left-steady uniform velocity profile, middle-steady parabolic velocity profile, right-pulsatile velocity profile.

surrounded by $r=r_0$, $z=0$, and $z=z_{max}$; the heating target (tumor and a part of blood vessel inside the tumor) is bounded by $r=r_1$, $z=z_1$, and $z=z_2$. The diameters of blood vessels and their associated average flow velocities considered in the current study are presented in Table I.

The governing equations for the temperature evolution are energy transport equations shown in Eqs. (8) for tissue and (9) for blood vessel:

$$\rho_t c_t \frac{\partial T_t}{\partial t} = k_t \left[\frac{1}{r} \frac{\partial}{\partial r} \left(r \frac{\partial T_t}{\partial r} \right) + \frac{\partial^2 T_t}{\partial z^2} \right] - W_b c_b (T_t - T_a) + Q_t(r, z, t), \tag{8}$$

$$\rho_b c_b \left(\frac{\partial T_b}{\partial t} + w \frac{\partial T_b}{\partial z} \right) = k_b \left[\frac{1}{r} \frac{\partial}{\partial r} \left(r \frac{\partial T_b}{\partial r} \right) + \frac{\partial^2 T_b}{\partial z^2} \right] + Q_b(r, z, t), \tag{9}$$

where $T(r, z, t)$ denotes the temperature that is distributed axis-symmetrically; ρ, k, c are density, thermal conductivity,

TABLE I. List of the blood vessel parameters used in current simulations (Ref. 8).

| Diameter (mm) | Average blood velocity in tumor (\bar{w}) (mm s ⁻¹) |
|---------------|---|
| 0.2 | 3.4 |
| 0.6 | 6 |
| 1.0 | 8 |
| 1.4 | 10.5 |
| 2.0 | 20 |

TABLE II. Three different heating schemes used in current simulations.

| Case | I | II | III |
|---|-----|-----|-----|
| Absorbed power density Q (W cm ⁻³) | 50 | 10 | 2 |
| Heating duration t_h (s) | 2 | 10 | 50 |
| Total absorbed energy density (J cm ⁻³) | 100 | 100 | 100 |

and specific heat, respectively, that are all assumed to be constant; $Q(r, z, t)$ is the power of heat added axis-symmetrically; W_b is the perfusion mass flow rate; T_a is the ambient temperature that is usually set to be 37 °C; $w(r, t)$ is that axial velocity of blood flow; subscripts t and b represent tissue and blood, respectively. Equation (8) is in fact Pennes' bioheat transfer equation³⁰ in cylindrical coordinates for tissue with the heat sink $-W_b c_b (T_t - T_a)$ to describe the perfusion effect by the network of microvascular blood flow. Equation (9) is the conventional energy transport equation for blood vessel with both convection and diffusion taken into account.

The initial condition is

$$T_t(r, z, 0) = T_b(r, z, 0) = T_a = 37 \text{ }^\circ\text{C}. \tag{10}$$

At the interface conditions between the blood vessel and tissue are continuity of temperature and heat flux

$$T_t = T_b \text{ at } \Gamma, \tag{11}$$

$$k_t \frac{\partial T_t}{\partial n} = k_b \frac{\partial T_b}{\partial n} \text{ at } \Gamma, \tag{12}$$

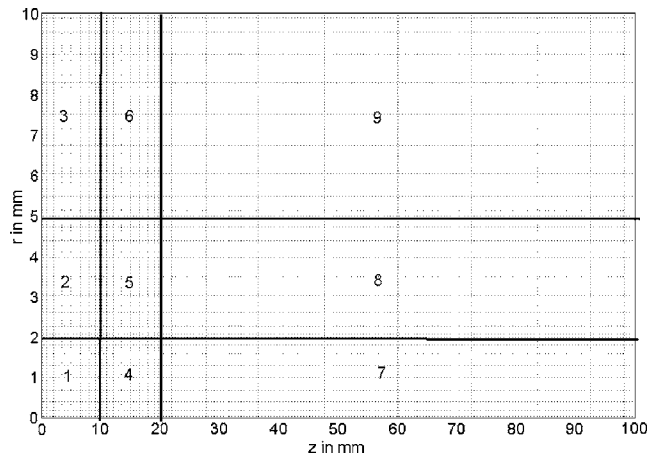


FIG. 3. The computational domain is decomposed into nine rectangular blocks. Blocks 1, 4, and 7 are blood vessel; block 5 is the tumor tissue; the other blocks are normal tissue. Blocks 4 and 5 are heating zone. Here the mesh resolution is 10×10 in each block. Due to the feature of Chebyshev collocation points, grids are clustered more densely near boundary/interface in each block. In this figure $r_{max}=10$ mm, $z_{max}=100$ mm, $r_0=2$ mm, $r_1=5$ mm, $z_1=10$ mm, $z_2=20$ mm.

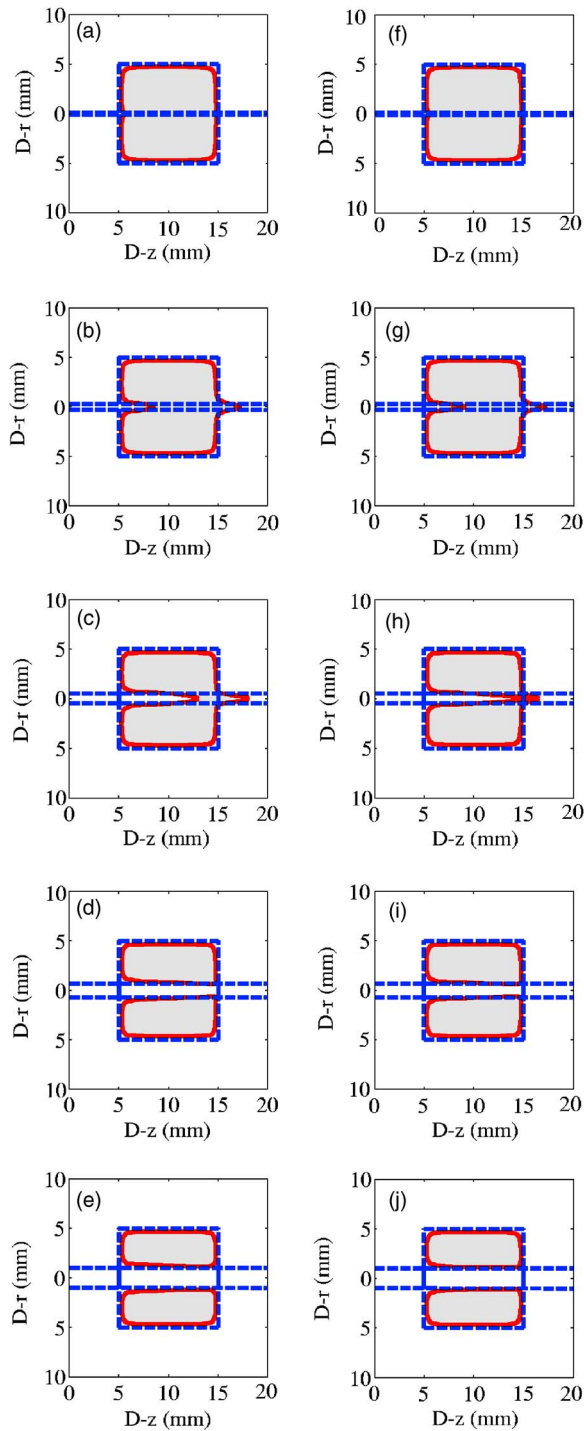


FIG. 4. Effect of the steady velocity profiles of blood flow on the thermal lesion region (shaded region) for the blood vessels: (a), (f) 0.2 mm; (b), (g) 0.6 mm; (c), (h) 1 mm; (d), (i) 1.4 mm; (e), (j) 2 mm in diameter. (a)–(e) are results of a uniform velocity profile, and (f)–(j) are results of a parabolic one. The blood vessel boundaries are denoted with the horizontal dashed lines. The heated target region (tumor) is denoted by a square with dashed lines. Here $r_1=5$ mm, $W_b=2$ kg m⁻³ s⁻¹, $\rho_b=\rho_t=1050$ kg m⁻³, $c_b=c_t=3770$ J kg⁻¹ °C⁻¹, $k_b=k_t=0.5$ W m⁻³ °C⁻¹. The target is heated in the way of the heating case I (i.e., $Q_t=Q_b=50$ W cm⁻³, and the heating duration = 2 s) in Table II.

where Γ denotes the interface between blood vessel and tissue, and n denotes the direction normal to Γ . At $r=0$, pole condition is applied for blood vessel by axis-symmetry,

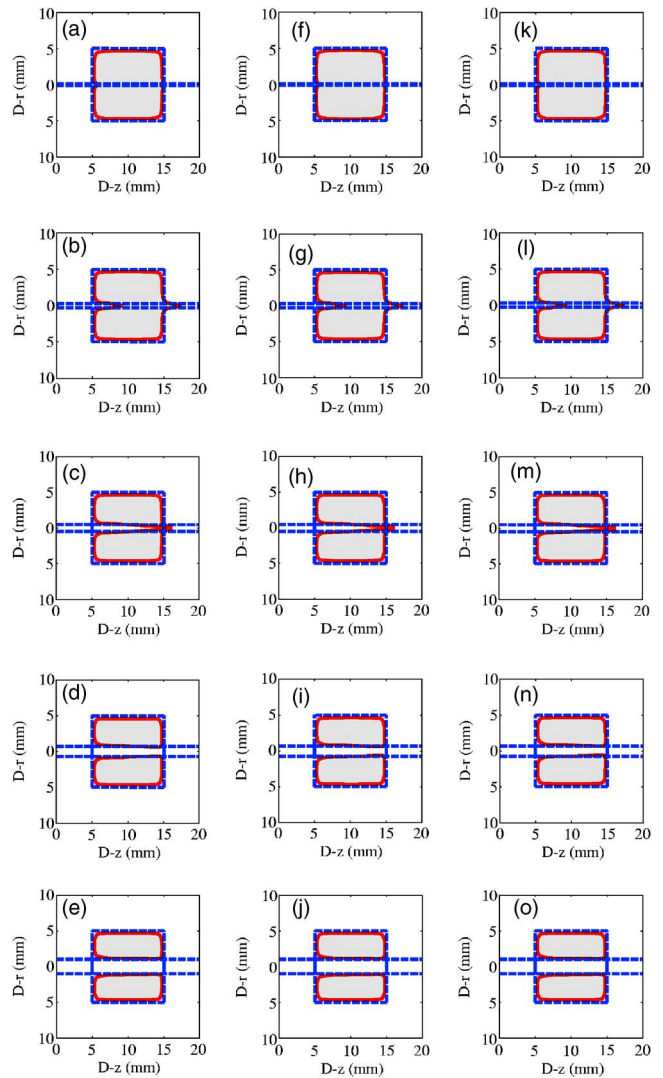


FIG. 5. Effect of the frequency of the pulsatile blood flow on the thermal lesion region (shaded region) for the blood vessels (a), (f), (k) 0.2 mm; (b), (g), (l) 0.6 mm; (c), (h), (m) 1 mm; (d), (i), (n) 1.4 mm; (e), (j), (o) 2 mm in diameter. (a)–(e) with the frequency 1 Hz, (f)–(j) with the frequency 1.5 Hz, and (k)–(o) with the frequency 2 Hz. The blood vessel boundaries are denoted with the horizontal dashed lines. The heated target region is denoted by a square with dashed lines. Here $r_1=5$ mm, $W_b=2$ kg m⁻³ s⁻¹, $\rho_b=\rho_t=1050$ kg m⁻³, $c_b=c_t=3770$ J kg⁻¹ °C⁻¹, $k_b=k_t=0.5$ W m⁻³ °C⁻¹. The target is heated in the way of the heating case I (i.e., $Q_t=Q_b=50$ W cm⁻³, and the heating duration = 2 s) in Table II.

$$\frac{\partial T_b}{\partial r} = 0. \tag{13}$$

Finally, the boundary condition at $r=r_{\max}$, $z=0$, and $z=z_{\max}$ is temperature all equal to the ambient one,

$$T_t \text{ (or } T_b) = T_a = 37 \text{ }^\circ\text{C}, \tag{14}$$

except the blood part at $z=z_{\max}$ using convective boundary condition,

$$\frac{\partial T_b}{\partial t} + w \frac{\partial T_b}{\partial z} = 0, \quad \text{at } z = z_{\max}. \tag{15}$$

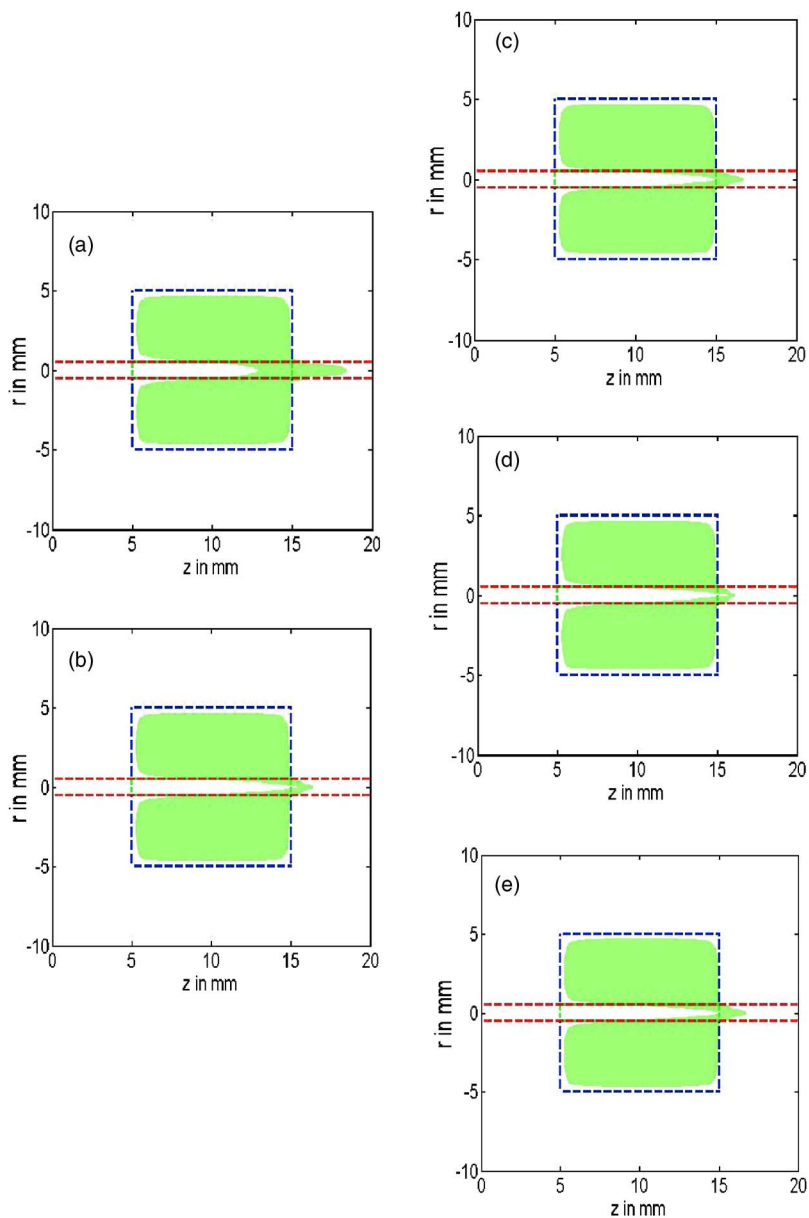


FIG. 6. Comparison of the effect of various velocity profiles on the thermal lesion region for 1-mm-diam blood vessel with (a) steady uniform velocity profile, (b) steady parabolic velocity profile, (c) 1 Hz and $fac=0.2$ pulsatile velocity profile, (d) 1.5 Hz and $fac=0.2$ pulsatile velocity profile, (e) 2 Hz and $fac=0.2$ pulsatile velocity profile.

C. Calculation of thermal dose

The accumulated thermal dose to tissue is a function of heating duration and the temperature level. The estimate of tissue damage is based on the thermal dose of which the formula was proposed by Sapareto and Dewey.³¹ The thermal dose or equivalent minutes at 43 °C (EM_{43}) is shown as follows:

$$EM_{43}(\text{in min.}) = \int_0^{t_f} R^{T-43} dt, \quad (16)$$

where $R=2$ for $T \geq 43$ °C, $R=4$ for 37 °C $< T < 43$ °C, and $t_f=90$ s or 120 s in current simulation. The threshold dose for necrosis is $EM_{43}=240$ min for muscle tissue.³² Therefore, the region encircled by the level curve $EM_{43}=240$ min is taken as the thermal lesion region in this study. Covering tumor tissue but not normal tissue by thermal lesion region as full as possible is most desired in the thermal treatment,

and the deficit would serve as an evaluation of the effectiveness of the treatment. This region is greatly influenced by size of blood vessel³¹ and the heating speed.³² Here three different heating schemes characterizing different heating speeds under the same amount of heat added (100 J cm^{-3} from preliminary energy analysis in lump³³) are depicted in Table II.

D. Numerical method

Here we used method of lines (MOL) to solve Eqs. (8)–(15). First, we employed multi-block Chebyshev pseudospectral method to discretize governing equations (8) and (9), boundary and interface conditions (10)–(15) in space into a semi-discrete system in time. This coupled system consists of ordinary differential equations in time, mainly from Eqs. (8) and (9), and algebraic equations, chiefly from boundary and interface conditions (10)–(15). We can then

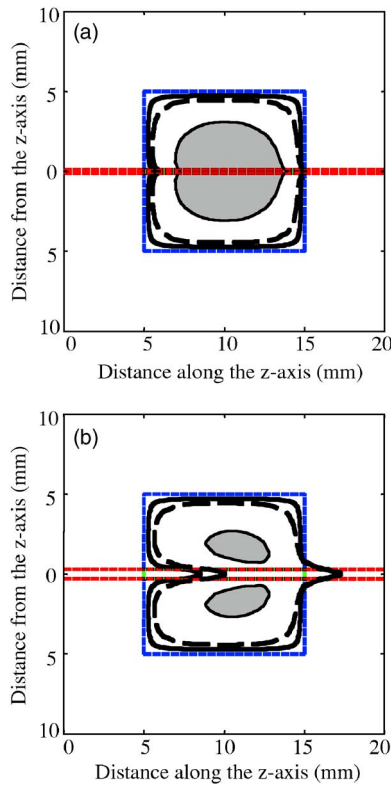


FIG. 7. Comparison of the effect of different heating schemes and blood vessel diameters on the thermal lesion region with steady uniform velocity profile. The solid and dashed lines represent the heating cases I and II, and the shaded area represents the heating case III. (a) The diameter of the blood vessel is 0.2 mm. (b) The diameter of the blood vessel is 1 mm.

solve this system of differential-algebraic equations (DAE's) by many efficient DAE solvers available from most numerical libraries, and here we used popular MATLAB index-1 DAE solver ode15s in our computation. Multi-block Chebyshev pseudospectral method first decomposes the computational domain into several blocks, based on heterogeneity of thermal properties or heating, and discretizes equations in space in each block by conventional Chebyshev pseudospectral method. Details about Chebyshev pseudospectral meth-

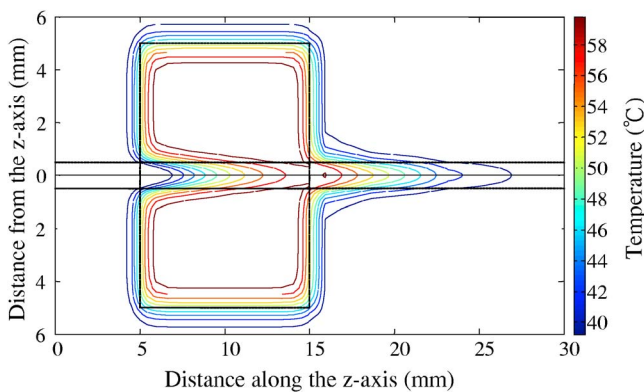


FIG. 8. The temperature contours for the case of blood vessel diameter 1 mm with steady uniform blood flow under case-I heating (i.e., $Q_t=Q_b=50 \text{ W cm}^{-3}$, and the heating duration=2 s) at the time of power off ($t=2 \text{ s}$) with the highest temperature reaching $62.108 \text{ }^\circ\text{C}$.

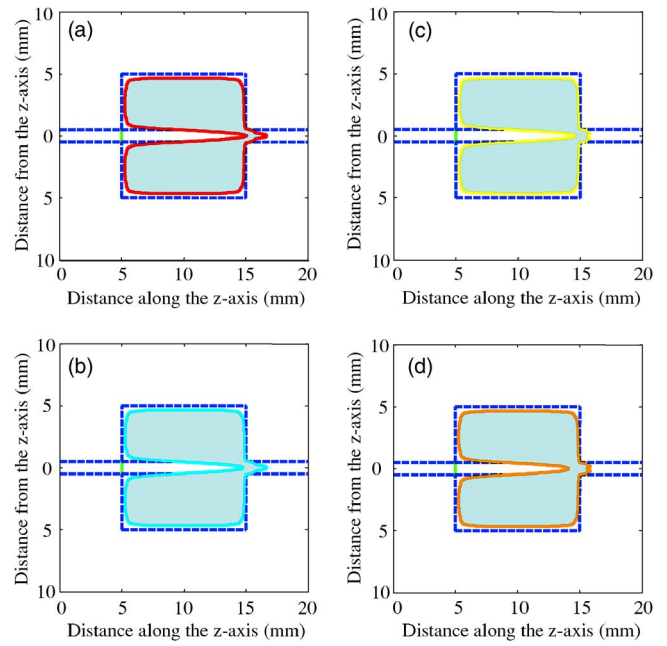


FIG. 9. Effect of *fac* of the pulsatile blood flow on the thermal lesion region with the pulsatile frequency being 1 Hz. The target is heated in the way of the heating case I (i.e., $Q_t=Q_b=50 \text{ W cm}^{-3}$, and the heating duration=2 s) in Table II. (a) *fac*=0.2, (b) *fac*=0.5, (c) *fac*=0.8, and (d) *fac*=1.

ods are referred to Canuto *et al.*,³⁴ Trefethen,³⁵ and Fornberg.³⁶ Here the computational domain is decomposed to nine rectangular blocks to cope with blood vessel and heating zone as shown in Fig. 3. We can observe from Fig. 3 that the grids are clustered more densely near boundary/

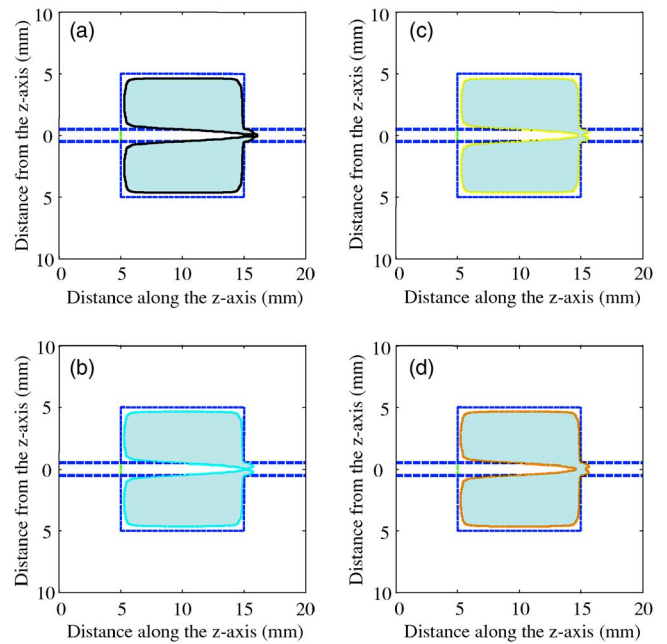


FIG. 10. Effect of *fac* of the pulsatile blood flow on the thermal lesion region with the pulsatile frequency being 1.5 Hz. The target is heated in the way of the heating case I (i.e., $Q_t=Q_b=50 \text{ W cm}^{-3}$, and the heating duration=2 s) in Table II. (a) *fac*=0.2, (b) *fac*=0.5, (c) *fac*=0.8, and (d) *fac*=1.

interface due to the characteristics of Chebyshev collocation points.^{34–36} This feature makes the computational accuracy and efficiency far better than the one without any decomposition. In short, owing to the intrinsic high order of accuracy of pseudospectral methods, grid size is not that restricted as finite difference/element methods and, hence, the overall computation is very efficient.

III. RESULTS AND DISCUSSIONS

Figure 4 compares the effects of steady uniform and parabolic velocity profiles for blood flow on thermal lesion region with heating scheme I in Table II, which has the least thermal dose deficit as described in Shih *et al.*⁹ Likewise, Fig. 5 compares the effects of pulsatile blood flow with various pulsatile frequencies (1, 1.5, and 2 Hz) with the relative intensity of pulsation $fac=0.2$ on thermal lesion region with heating Scheme I in Table II. Figures 4 and 5 generally show that there is almost no difference in thermal lesion region among all these velocity profiles under the same size of blood vessel. Only minor difference of thermal lesion region in blood vessel is observed in middle-sized blood vessels (with diameter 0.6 and 1 mm). This minor difference is most pronounced for blood vessel of diameter 1 mm and is particularly shown in Fig. 6. It shows that the length of thermal lesion region in blood vessel is longest for uniform velocity profile, shortest for parabolic and 1.5 Hz pulsatile ones, and in between for 1 and 2 Hz pulsatile flows.

While the thermal lesion region is rather insensitive to the velocity profile of blood flow, it is deeply influenced by the size of blood vessel since the heat convection by the blood flow in a blood vessel usually serves as a stronger heat sink than the blood perfusion in tissue. That means temperature would drop faster in a blood vessel than its surrounding tissue. This may cause deficit of thermal lesion region in blood vessel and tissue nearby, which can be easily observed from Figs. 4 and 5. Generally the deficit of thermal lesion region is less for smaller vessels. In the case of smallest vessel here (with diameter 0.2 mm), thermal lesion region almost covers the whole blood vessel inside the tumor and the deficit is naturally the least. For middle-sized vessels here (with diameter 0.6 and 1 mm), the thermal lesion region in blood vessel becomes smaller and shifted downstream. For large vessels here (with diameter 1.4 and 2 mm), there is a total deficit of thermal lesion region in blood vessel, and this would cause deficit in tumor tissue right near the blood vessel especially at the upstream.

Besides diameters of blood vessel, the thermal lesion region is also very sensitive to the heating speed. Figure 7 generally shows larger thermal lesion region for faster heating, and the heating speed affects more pronouncedly when the blood vessel is larger. As shown in Fig. 7(b), there exists an obvious shift of thermal lesion region to the downstream of blood vessel for the blood vessel with diameter 1 mm when heating is fast, and this may cause unwanted thermal injury in normal tissue nearby. Figure 8 particularly shows the temperature contours for the case of blood vessel diameter of 1 mm under heating Scheme I in Fig. 7 at the time of

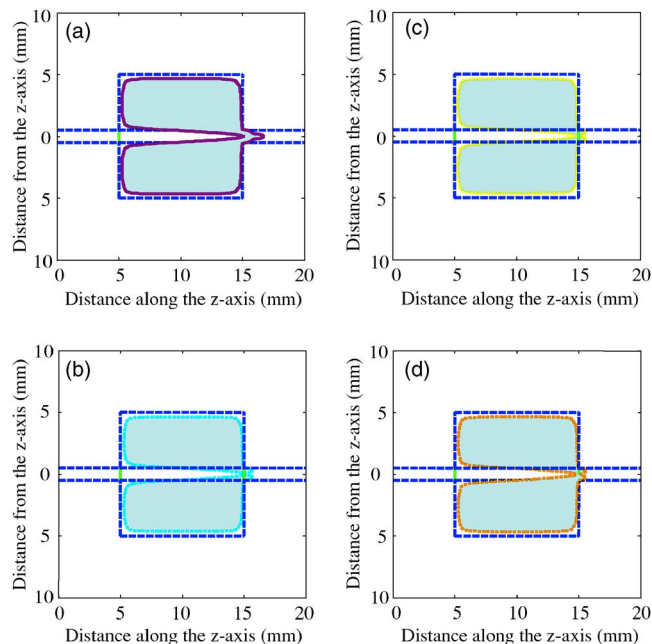


FIG. 11. Effect of fac of the pulsatile blood flow on the thermal lesion region with the pulsatile frequency being 2 Hz. The target is heated in the way of the heating case I (i.e., $Q_t=Q_b=50 \text{ W cm}^{-3}$, and the heating duration=2 s) in Table II. (a) $fac=0.2$, (b) $fac=0.5$, (c) $fac=0.8$, and (d) $fac=1$.

power off ($t=2 \text{ s}$). Notice that the highest temperature occurs right at the downstream of blood vessel. This causes the thermal damage of the normal tissue nearby.

The effect of pulsation amplitude, in terms of relative intensity fac , of pulsatile blood flow on the thermal lesion region generally has little difference among various fac 's, except minor difference for middle-sized blood vessels. Figures 9–11 depicts this effect for a middle-sized blood vessel of diameter 1 mm with $fac=0.2$, 0.5, 0.8, and 1 and frequency being at 1 Hz (Fig. 9), 1.5 Hz (Fig. 10), and 2 Hz (Fig. 11), respectively. When fac increases, the blood flows more in a stick-slip fashion, and this may considerably influence the heat convection when incorporated with pulsation frequency. Figures 9, 10, 11(c), and 11(d), with $fac=0.8$ and 1, respectively, show obviously two-peak behavior in thermal dose contour at the downstream of blood vessel, which is chiefly because of large pulsation amplitude.

IV. CONCLUSION

The current investigation shows that the effect of velocity profile of blood flow, ranging from uniform, parabolic, to pulsatile ones, has almost no difference in thermal lesion region on tumor region and minor difference only on blood vessel when the blood vessel is of middle size. This result suggests that we might just as well use the simplest steady uniform velocity profile to do the simulation without significant difference in thermal lesion region of tumor. In fact, the thermal lesion region is much more sensitive to heating speed and size of blood vessel. Some studies^{8,9,26,33} show that faster heating would form a much better thermal lesion

region, and it works best on small blood vessels with a better covering of both the tumor and blood vessel by the thermal lesion region since the heat convection by the blood flow in the blood vessel is least. For large vessels, it has a total deficit in blood vessel and some deficit in tumor near the upstream of blood vessel. As to middle-sized vessels, a shift of partially deficient thermal lesion region to the downstream of blood vessel may cause unwanted thermal injury to the normal tissue nearby. Furthermore, for middle-sized blood vessels, pulsatile blood flow of large pulsation amplitudes may further cause a two-peak behavior in the thermal dose contour at the downstream of blood vessel.

ACKNOWLEDGMENT

This research was supported in part by the National Science Council of the Republic of China under Grant No. NSC-94-2213-E-039-004.

- ^{a)} Author to whom correspondence should be addressed. Electronic mail: shih@mail.cmu.edu.tw
- ¹J. Crezee and J. J. W. Lagendijk, "Experimental verification of bioheat transfer theories: measurement of temperature profiles around large artificial vessels in perfused tissue," *Phys. Med. Biol.* **35**, 905–923 (1990).
 - ²W. M. Whelan, D. R. Wyman, and B. C. Wilson, "Investigations of large vessel cooling during interstitial laser heating," *Med. Phys.* **22**, 105–115 (1995).
 - ³M. C. Kolios, M. D. Sherar, and J. W. Hunt, "Large blood vessel cooling in heated tissues: A numerical study," *Phys. Med. Biol.* **40**, 477–494 (1995).
 - ⁴M. C. Kolios, A. E. Worthington, M. D. Sherar, and J. W. Hunt, "Experimental evaluation of two simple thermal models using transient temperature analysis," *Phys. Med. Biol.* **43**, 3325–3340 (1998).
 - ⁵C. X. Zhang, S. Zhang, Z. Zhang, and Y. Z. Chen, "Effects of large blood vessel locations during high intensity focused ultrasound therapy for hepatic tumors: a finite element study," *Proceeding of the 2005 IEEE Engineering in Medicine and Biology 27th Annual Conference*, Shanghai, China, 1–4 September 2005.
 - ⁶M. Nikfarjam, V. Muralidharan, C. Malcontenti-Wilson, W. McLaren, and C. Christophi, "Impact of blood flow occlusion on liver necrosis following thermal ablation," *ANZ J. Surg.* **76**, 84–91 (2006).
 - ⁷S. M. Becker and A. V. Kuznetsov, "Numerical modeling of in vivo plate electroporation thermal dose assessment," *ASME J. Biomech. Eng.* **128**, 76–84 (2006).
 - ⁸T. C. Shih, H. S. Kou, and W. L. Lin, "The impact of thermally significant blood vessels in perfused tumor tissue on thermal distributions during thermal therapies," *Int. Commun. Heat Mass Transfer* **30**, 975–985 (2003).
 - ⁹T. C. Shih, H. L. Liu, and A. T. L. Horng, "Cooling effect of thermally significant blood vessels in perfused tumor tissue during thermal therapy," *Int. Commun. Heat Mass Transfer* **33**, 135–141 (2006).
 - ¹⁰L. E. Fencil, K. Doi, K. G. Chua, and K. R. Hoffman, "Measurement of absolute flow rate in vessels using a stereoscopic DSA system," *Phys. Med. Biol.* **34**, 659–671 (1989).
 - ¹¹W. W. Nichols and M. F. O'Rourke, *McDonald's Blood Flow in Arteries: Theoretic, Experimental and Clinical Principles* (Edward Arnold, London, 1990).
 - ¹²Y. C. Fung, *Biomechanics: Motion, Flow Stress, and Growth* (Springer-Verlag, New York, 1996).
 - ¹³D. K. De, "Theoretical investigation of estimation of steady and pulsatile blood flow and blood vessel cross section by CW NAR excitation," *Phys. Med. Biol.* **35**, 197–211 (1990).
 - ¹⁴D. N. Ku, "Blood flow in arteries," *Annu. Rev. Fluid Mech.* **29**, 399–434 (1997).
 - ¹⁵O. I. Craciunescu and S. T. Clegg, "Pulsatile blood flow effects on temperature distribution and heat transfer in rigid vessels," *J. Biomech. Eng.* **123**, 500–505 (2001).
 - ¹⁶M. B. Robertson, U. Köhler, P. R. Hoskins, and I. Marshall, "Flow in elliptical vessels calculated for a physiological waveform," *J. Vasc. Res.* **38**, 73–82 (2001).
 - ¹⁷B. Smith, J. G. Chase, R. I. Nokes, G. M. Shaw, and T. David, "Velocity profile method for time varying resistance in minimal cardiovascular system models," *Phys. Med. Biol.* **48**, 3375–3387 (2003).
 - ¹⁸L. Yao, D. Liao, Y. Zeng, X. Xu, and H. Xu, "Radial distributions of temperature pressure and velocities for pulsatile blood flow in an axisymmetrical stiff tube," *Physiol. Meas.* **25**, 1437–1442 (2004).
 - ¹⁹Y. J. Zeng, J. H. Zhang, B. Shen, Y. Diao, X. H. Xu, and H. Xu, "Measuring blood flow velocities based on three image processing techniques," *Med. Phys.* **32**, 1187–1192 (2005).
 - ²⁰J. R. Womersley, "Method for the calculation of velocity, rate of flow and viscous drag in arteries when the pressure gradient is known," *J. Physiol. (London)* **127**, 553–563 (1955).
 - ²¹C. Loudon and A. Tordesillas, "The use of the dimensionless Womersley number to characterize the unsteady nature of internal flow," *J. Theor. Biol.* **191**, 63–78 (1998).
 - ²²A. Kotte, G. van Leeuwen, J. de Bree, J. van der Koijk, H. Crezee, and J. Lagendijk, "A description of discrete vessel segments in thermal modeling of tissues," *Phys. Med. Biol.* **41**, 865–884 (1996).
 - ²³J. C. Chato, "Heat transfer to blood vessels," *J. Biomech. Eng.* **102**, 110–118 (1980).
 - ²⁴J. J. W. Lagendijk, "The influence of bloodflow in large vessels on the temperature distribution in hyperthermia," *Phys. Med. Biol.* **27**, 17–23 (1982).
 - ²⁵J. Crezee and J. J. W. Lagendijk, "Temperature uniformity during hyperthermia: the impact of large vessels," *Phys. Med. Biol.* **37**, 1321–1337 (1992).
 - ²⁶M. C. Kolios, M. D. Sherar, and J. W. Hunt, "Blood flow cooling and ultrasonic lesion formation," *Med. Phys.* **23**, 1287–1298 (1996).
 - ²⁷L. Consiglieri, I. dos Santos, and D. Haemmerich, "Theoretical analysis of the heat convection coefficient in large vessels and the significance for thermal ablative therapies," *Phys. Med. Biol.* **48**, 4125–4134 (2003).
 - ²⁸Y. Mohammed and J. F. Verhey, "A finite element method model to simulate laser interstitial thermo therapy in anatomical inhomogeneous regions," *Biomed. Eng. Online* **4**, 1–16 (2005).
 - ²⁹Y. C. Fung, *Biomechanics: Circulation* (Springer-Verlag, New York, 1996).
 - ³⁰H. H. Pennes, "Analysis of tissue and arterial blood temperature in the resting human forearm," *J. Appl. Physiol.* **1**, 93–122 (1948).
 - ³¹S. A. Sapareto and W. C. Dewey, "Thermal dose determination in cancer therapy," *Int. J. Radiat. Oncol., Biol., Phys.* **10**, 787–800 (1984).
 - ³²C. Damianou and K. Hynynen, "Focal spacing and near-field heating during pulsed high temperature ultrasound therapy," *Ultrasound Med. Biol.* **19**, 777–787 (1993).
 - ³³H. S. Kou, T. C. Shih, and W. L. Lin, "Effect of the directional blood flow on thermal dose distribution during thermal therapy: An application of a Green's function based on the porous model," *Phys. Med. Biol.* **48**, 1577–1589 (2003).
 - ³⁴C. Canuto, M. Y. Hussaini, A. Quarteroni, and T. A. Zang, *Spectral Methods, Fundamentals in Single Domains* (Springer-Verlag, Berlin, Heidelberg, 2006).
 - ³⁵L. N. Trefethen, *Spectral Methods in MATLAB* (SIAM, Philadelphia, 2000).
 - ³⁶B. Fornberg, *A Practical Guide to Pseudospectral Methods* (Cambridge University Press, Cambridge, 1996).